Journal of Power Sources 220 (2012) 211–216

Contents lists available at SciVerse ScienceDirect

Journal of Power Sources

journal homepage: www.elsevier.com/locate/jpowsour

Short communication

Gold–Palladium nanoparticles supported by mesoporous β-MnO_2 air electrode for rechargeable Li-Air battery

Arjun Kumar Thapa [a,b,*], Tae Ho Shin [b], Shintaro Ida [b], Gamini U. Sumanasekera [a], Mahendra K. Sunkara [a], Tatsumi Ishihara [b]

[a] Conn Center for Renewable Energy Research, University of Louisville, 216 Ernst Hall, Louisville, KY 40292, USA
[b] Department of Applied Chemistry, Kyushu University, 744 Moto oka, Nishi ku, Fukuoka 819-0395, Japan

HIGHLIGHTS

- Au/Pd NPs supported mesoporus β-MnO_2 air electrode was synthesized by hydrothermal process.
- Au/Pd NPs supported mesoporus β-MnO_2 air electrode has a high discharge capacity of 775 mAh g^{-1}.
- *Ex-situ* XRD and Raman spectroscopy measurements confirm the Li_2O_2 formation during discharge.
- A stable cycle performance of Li-Air battery is attributed to the catalytic effect of Au–Pd on mesoporus β-MnO_2.

ARTICLE INFO

Article history:
Received 25 May 2012
Received in revised form
16 July 2012
Accepted 1 August 2012
Available online 9 August 2012

Keywords:
Gold–Palladium nanoparticles
Mesoporous β-MnO_2
Raman spectroscopy
Ex-situ XRD
Li-Air battery

ABSTRACT

The electrochemical performance and electrode reaction using Au–Pd nanoparticle (NP) supported mesoporous β-MnO_2 as a cathode catalyst for rechargeable Lithium-Air (Li-Air) battery is reported here for the first time. In this study, Au–Pd NP-supported mesoporous β-MnO_2 was successfully synthesized by hydrothermal process using a silica KIT-6 template. It has an initial discharge capacity of ca. 775 mAh g^{-1} with high reversible capacity at a current density of 0.13 mA cm^{-2}. The Au–Pd NP-supported mesoporous β-MnO_2 cathode catalyst, which enhances the kinetic of oxygen reduction and evolution reactions (ORR/OERs), thereby improves energy and coulombic efficiency of the Li-Air cell. Raman spectroscopy and *ex-situ* XRD results of the Au–Pd NP-supported mesoporous β-MnO_2 air electrode suggest that the observed capacity comes from oxidation of Li^+ to form Li_2O_2 during discharge to 2.0 V.

1. Introduction

Lithium-air (Li-Air) batteries have been attracting recent worldwide research attention due to their relatively high specific capacity and high energy density. In a conventional non-aqueous Li-Air battery, the Li anode is electrochemically coupled to atmospheric oxygen through an air cathode. During discharge, Li^+ reacts with O_2 at the cathode to form Li_2O_2 or Li_2O. During the charge process, these Li_2O_2 or Li_2O products decompose to Li^+ and O_2. In 1991, Abraham and Jiang first reported the Li-Air battery using a non-aqueous electrolyte [1]. They suggested that during discharge, Li^+ reacts with O_2 to form Li_2O_2 as a discharge product, which precipitates in the pores of porous carbon-based air electrodes and blocks further intake of oxygen to abruptly terminate the discharge reaction. Based on oxygen consumption measurements, Read et al. suggested that there are also other types of reactions occurring during discharge, i.e., $4(Li^+ + e^-) + O_2 - 2Li_2O$ [2,3]. In 2006, Bruce et al. reported a Li-Air battery using MnO_2 catalysts [4–6]. They showed the high capacity for the Li-Air battery with good cycle stability up to 50 cycles. Recently, Mizuno et al. reported that a Li-Air battery using propylene carbonate (PC) containing EC600JD ketjen black carbon and MnO_2 catalysts had an initial discharge capacity of more than 800 mAh g^{-1} and retained 60% of its initial capacity after 100 cycles at a current density of 0.025 mA cm^{-2} [7]. Recently, a Li-Air battery was reported using the MnO_2 catalyst [8]. MnO_2 can be favorably used as an electro catalyst for oxygen reduction and evolution reactions (ORR/OERs) due to its low cost and low toxicity [9–11]. Here, we report for the first time

* Corresponding author. Conn Center for Renewable Energy Research, University of Louisville, 216 Ernst Hall, Louisville, KY 40292, USA. Tel.: +1 502 852 4123; fax: +1 502 852 8619.
E-mail addresses: akthap01@louisville.edu, arjun557@hotmail.com (A.K. Thapa).

0378-7753/$ – see front matter © 2012 Elsevier B.V. All rights reserved.
http://dx.doi.org/10.1016/j.jpowsour.2012.08.003

that a Li-Air battery using Pd–Au nanoparticle (NP)-supported mesoporous β-MnO_2 electrode, which enhances the kinetic of the ORR/OER due to the increase in catalytic activity of the air electrode, thereby improves the energy and coulombic efficiency of the cell.

2. Experimental condition

2.1. Synthesis of materials

Pluronic P123 has been widely used as a typical mesostructural template for the synthesis of mesoporous silica and carbon [12,13]. The mesoporous silica KIT-6 was synthesized using a 100 °C hydrothermal treatment following a previously reported procedure [14,15]. A 10 g quantity of the co-polymer P123 surfactant was mixed with 34.94 mL of distilled water and 16 mL of concentrated HCl (36%). After stirring the mixture at 25 °C until homogeneous, 10 g of *n*-butanol (99.5%) was added, stirred for 1 h, and combined with 21.5 g of tetra ethyl orthosilicate (98%). After stirring at 35 °C for 24 h, the mixture was heated in an autoclave at 100 °C for 24 h. The precipitate was filtered, dried at 60 °C, and then added to 300–400 mL of ethanol and 20–30 mL of concentrated HCl (36%). Following 1–2 h stirring, the mixture was filtered, washed several times with ethanol and water, and dried again at 60 °C. The resulting mesoporous solid was calcined at 500 °C for 3 h in air. The sample was denoted as KIT-6 template.

The Au–Pd NP-loaded mesoporous β-MnO_2 with a regular shape was synthesized using mesoporous silica KIT-6 as a template. In typical synthesis of Au–Pd NP-supported β-MnO_2, 75.1 mg of $HAuCl_4$ and 32.4 mg of accurately weighed $PdCl_2$ were poured in a beaker containing 15 mL of ethanol and stirred continuously while adding 3 to 5 drops of 0.2 M dilute HCl solution to dissolve Pd and change the hydrosol from a light purple to a dark brown solution. Exactly 0.3 g of $Mn(NO_3)_2 \cdot 6H_2O$ was then poured in the same beaker and stirred continuously until the solution became transparent. Next, 0.3 g of silica KIT-6 template was poured into the same beaker. The solution was continuously stirred at room temperature until all the solution was absorbed. After collecting the entire precursor, it was heated to 350 °C at the rate of 1° min^{-1} for 5 h. The sample was then treated with hot 2 M NaOH to remove the silica KIT template. Finally, the sample was washed thoroughly with water several times and dried at 60 °C for 12 h.

2.2. Characterization of samples

The Au–Pd NP-supported mesoporous β-MnO_2 powder was characterized by a combination of techniques including: X-ray diffraction (XRD, Rigaku Rint 2500); scanning electron microscopy (SEM, Keyence 8100); transmission electron microscopy (TEM; JEM 2100); high resolution (HR) TEM (JEOL 2010); Brunauer, Emmett, and Teller (BET) surface area (Nippon Bell, BELSORP 18PLUS-FS); and Raman spectroscopy measurements (Horiba Jobin Yvon HR800).

Powder XRD was carried out by using a Rigaku Rint 2500HLR diffractometer with CuKα radiation at the low-angle scanning range of 0.5–10° and the wide-angle range of 10–80° (2θ). Nitrogen adsorption–desorption isotherm was measured using a Bell Japan (Bell Mini) instrument and the specific surface area was calculated by the BET method. The particle morphologies of the resulting Au–Pd NP-supported mesoporous β-MnO_2 compounds were observed by SEM, (Keyence VE-7800). TEM (JEM 2100) and HRTEM observations were performed using a JEOL JEM-2010 electron microscope. Raman spectroscopy was carried out using a Horiba Jobin Yvon HR800 with 744 nm initial excitation laser.

2.3. Electrochemical measurements

The electrochemical characterizations were carried out using Swagelok type cell. The cathode was formed by casting a mixture of Au–Pd NP-supported mesoporous β-MnO_2, and polytetrafluroethylene (PTFE)-coated teflonized acetylene black (TAB-2) as a conducting binder (mol ratio of 90:10); this mixture was pressed onto a stainless steel mesh and the cathode was dried at 160 °C for 12 h under vacuum.

Li-Air cell measurements were carried out at room temperature. The Li-Air battery configuration used in this study consisted of a lithium foil (12 mm in diameter) used as an anode electrode that was separated by two pieces of porous polypropylene film (Celgard 3401). The cell was gas tight except for the stainless steel mesh window that exposed the porous cathode to O_2 atmosphere. The electrolyte used was 1 M LiTFSI-EC:DEC lithium bis(trifluoromethanesulfonyl)imide-ethylene carbonate: diethyl carbonate (3:7 by volume), which was supplied by Ube Chemical Co. Ltd., Japan. Charge–discharge performance was carried out at the voltage range of 4.0–2.0 V at the current densities of 0.13, 0.63, 1.91, and 2.55 mA cm^{-2}, respectively. The observed capacity was normalized by the total weight of the air electrode, but not with the weight of carbon for capacity comparison in this study. Although, a practical Li-Air battery can be tested in an open-air operational environment since the moisture content in the air will react with lithium negative electrode, and CO_2 will consume lithium salts in the electrolyte. To avoid these negative effects, the cell was enclosed and tested in a 1 atm dry pure oxygen environment.

Examination of the discharged electrode involves disassembly of the cell in a controlled argon atmosphere glove box, rinsing the cathode electrode with diethyl carbonate, removing the solvent under vacuum, and then placing the electrode in an air tight holder.

3. Results and discussion

The low-angle XRD data for Au–Pd NP-supported mesoporous β-MnO_2 are shown in Fig. 1(a). The sharp diffraction intensity peak was observed at 1.02°, suggesting the formation of mesoporous structure. Wide-angle XRD patterns of as-prepared Au–Pd NP-supported mesoporous β-MnO_2 and mesoporous β-MnO_2 powders are shown in Fig. 1(b). Previously, we successfully synthesized mesoporous β-MnO_2 powders using a hydrothermal process [11]. In this study, we loaded bimetallic Au and Pd on mesoporous β-MnO_2 using a hydrothermal reaction. Here, we show that loading of Au and Pd leads to a shift in the diffraction peak of β-MnO_2 powder. The XRD pattern of the sample found at 38.2°, 44.3°, 64.6°, 77.6°, and 81.6° are characteristic of gold NPs. From these XRD patterns of Au–Pd NP-supported mesoporous β-MnO_2, it can be seen that β-MnO_2 shows sharp intensity peaks at various 2θ angles with a highly crystalline pure β-MnO_2 phase.

Fig. 2a shows the SEM image of Au and Pd loaded β-MnO_2. From the SEM image of Au–Pd-loaded mesoporous β-MnO_2, it can be seen that small NPs were aggregated to form large secondary particles of about 5–10 nm. Fig. 2b shows the TEM image of bimetallic Au–Pd NP-supported mesoporous β-MnO_2. From this TEM image, it is clearly seen that the Au NPs are brighter, owing to their heavier atomic weight, whereas Pd NPs are darker. The Pd NPs are 5–6 nm in diameter while Au NPs are small round particles of about 3–4 nm, which are uniformly distributed within the particles of the mesoporous β-MnO_2. The high resolution (HR) TEM image shown in Fig. 2c, provides further evidence of successful loading of the Au and Pd NPs on mesoporous β-MnO_2.

Fig. 3a shows the N_2 adsorption/desorption isotherms curve of Au–Pd NP-supported mesoporous β-MnO_2. This N_2 adsorption/desorption isotherm curve shows a typical IV type H_1 hysteresis loop, which is characteristic of the mesoporous structure. The BET

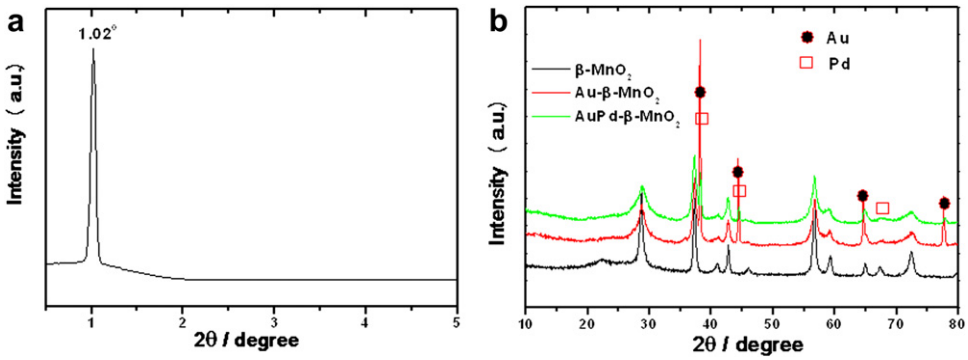

Fig. 1. (a) Low-angle and (b) wide-angle XRD pattern of Au–Pd NP-supported mesoporous β-MnO_2.

surface area of Au–Pd NP-supported mesoporous β-MnO_2 is 47.5 m^2 g^{-1}. The pore size distribution of Au–Pd NPs-supported mesoporous β-MnO_2 is shown in Fig. 3b. The pore size distribution calculated from the desorption branch of the isotherms was narrow and centered on a diameter of 3.09 nm with a pore volume of 0.31 cm^3 g^{-1}.

We investigated the charge/discharge measurement of Pd/mesoporous β-MnO_2 and Au–Pd NP-supported mesoporous β-MnO_2 air electrodes for the Li-Air battery at a voltage range of 4.0–2.0 V with a current density of 0.13 mA cm^{-2} as shown in Fig. 4(a) and (b). The mesoporous β-MnO_2/Pd electrode had an initial discharge capacity of 576 mAh g^{-1} during the first cycle. During discharge, a small plateau at 2.9 V vs. Li/Li^+ and a large plateau around 2.7 V vs. Li/Li^+, were observed. However, during the charge process, a small plateau at 3.1 V vs. Li/Li^+ and a large plateau 3.7 V vs. Li/Li^+ with high reversible capacity were observed. The Au–Pd NP-supported mesoporous β-MnO_2 air electrode has an initial discharge capacity of 775 mAh g^{-1} during the first cycle as shown in Fig. 4(b). With the loading of Au–Pd NPs on the mesoporous β-MnO_2 air electrode, the discharge capacity was drastically increased to more than ca. 200 mAh g^{-1}. The discharge voltage plateau was large and flat at 2.8 V vs. Li/Li^+, which is close to the theoretical potential of 2.95 V vs. Li/Li^+ for Li_2O_2 formation. The charging potential was observed at 3.6 V vs. Li/Li^+ with a high reversible capacity. Further charge/discharge measurements show the stable charge/discharge capacity of 714 mAh g^{-1} with a small degradation of capacity after 12 cycles. These charge/discharge potential curves of Au–Pd NP-supported meoporous β-MnO_2 electrode for the Li-Air battery show the energy efficiency of charge and discharge increases from 57% to 75.3%. Therefore, loading of Au–Pd NPs on the mesoporous β-MnO_2 electrode is effective for decreasing the charge potential to its theoretical value.

Some research groups like Mizuno and McCloskey et al. [7,16] reported Li_2CO_3 formation during the charge/discharge using 1 M

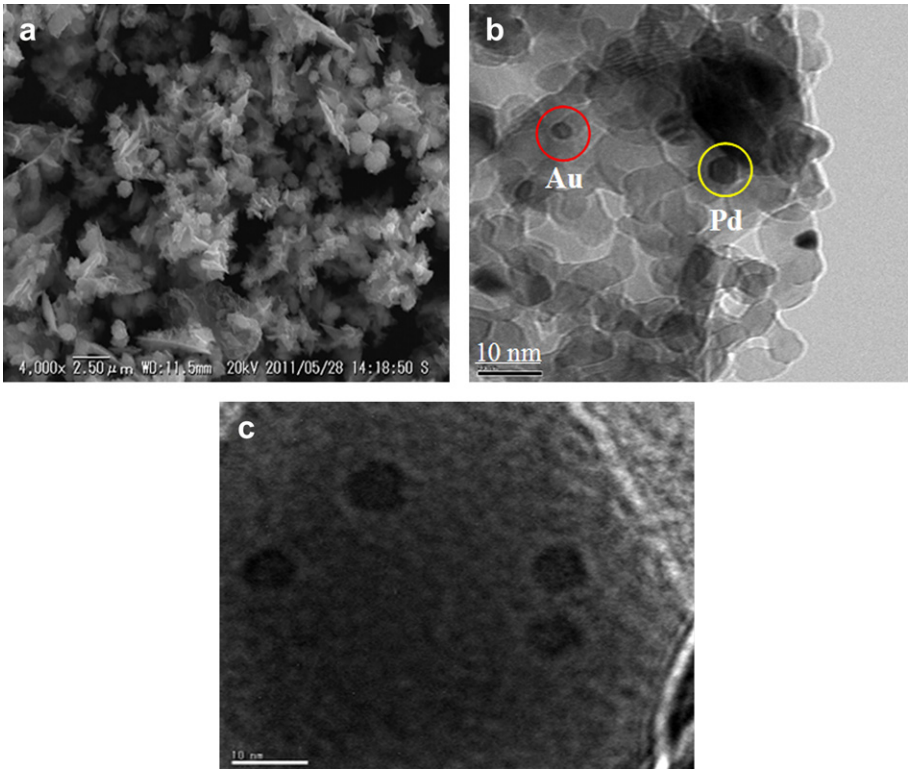

Fig. 2. (a) SEM image, (b) TEM image, and (c) High resolution (HR) TEM image of Au–Pd NP-supported mesoporous β-MnO_2.

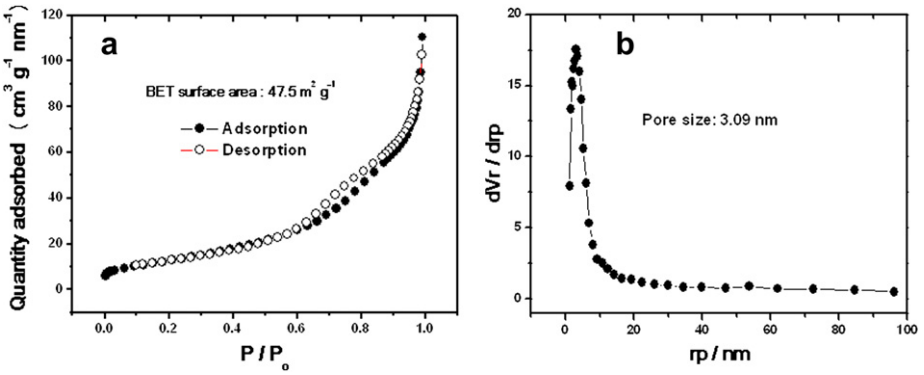

Fig. 3. (a) Nitrogen adsorption/desorption isotherms curve, and (b) pore size distribution of Au–Pd NP-supported mesoporous β-MnO_2.

$LiPF_6$-PC based electrolyte. In this study, the electrolyte used was 1 M LiTFSI-EC:DEC (3:7), which is well known as being more stable and safe compared to $LiPF_6$ [17], especially when electrochemical windows between 2.0 and 4.0 V are applied and when small amount of teflonized acetylene black binder are used in the air electrode. This result suggested that the Au–Pd NP-supported meoporous β-MnO_2 electrode shows negligible Li_2CO_3 formation during charge/discharge. One reason for negligible Li_2CO_3 formation was that the charging potential was limited to 4.0 V and a small amount of (TAB-2) binder was used as air electrode. The results from other groups indicate that large amounts of carbon were used for the air electrode. In our previous report, we found that the MnO_2 electrode without carbon shows high reversibility without forming Li_2CO_3 [9]. This is important for the reversibility of the Li-Air battery.

Fig. 5 shows the capacity as a function of cycle number for Au–Pd NP-supported β-MnO_2 air electrode for the Li-Air battery at the voltage range of 2.0–4.0 V with a current density of 0.13 mA cm^{-2}. It shows the initial discharge capacity of 775 mAh g^{-1} during the first cycle. In this study, a stable charge/discharge capacity of 714 mAh g^{-1} over 12 cycles and a small degradation during the cycling was observed. This result suggested that the Au–Pd NP-supported mesoporous β-MnO_2 electrode enhances the kinetic of the ORR/OER due to the increase in catalytic activity of the air electrode, which thereby improves the energy and coulombic efficiency of the cell. The capacity retention rate was 92.1% at a current density of 0.13 mA cm^{-2} after 12 cycles.

The rate property of the current Li-Air battery is generally not so good; they show large capacities only at low current densities. However, if the air catalyst is highly active, then a reasonably high capacity can be expected. Here, we also studied the rate property of the Au–Pd NP-supported mesoporous β-MnO_2 air cathode electrode for the Li-Air battery. The first charge discharge capacities vs. different current densities of the Au–Pd NP-supported mesoporous β-MnO_2 air electrode for the Li-Air battery as shown in Fig. 6 were 0.13, 0.63, 1.91, and 2.55 mA cm^{-2}. This shows the discharge capacities of 775, 545, 259, and 169 mAh g^{-1} at current densities of 0.13, 0.63, 1.91, and 2.55 mA cm^{-2}, respectively. The capacity retention rate was 70.3, 33.4, and 21.8% to the initial capacity at 0.63, 1.91, and 2.55 mA cm^{-2}, respectively. These results confirmed that the Au–Pd NP-supported mesoporous β-MnO_2 air electrode shows good performance, even when applying high current densities.

Fig. 7 shows the *ex-situ* XRD measurements of the Au–Pd NP-supported mesoporous β-MnO_2 electrode before discharge and after discharge to 200, 400 mAh g^{-1}, and 2.0 V vs. Li/Li^+, respectively. We studied the *ex-situ* XRD to determine what kinds of reactions occur during the discharge at these potentials. Before discharge, *ex-situ* XRD of Au–Pd NP-supported β-MnO_2 shows the peaks from each component. After discharge to 200 mAh g^{-1}, XRD patterns of Au–Pd NP-supported mesoporous β-MnO_2 show a new peak at 25.4°, which corresponds to the TAB-2 binder peak, while a shoulder-like peak appears near 35.0° and corresponds to the formation of Li_2O_2 during the initial discharge process. After discharge to 400 mAh g^{-1}, Au–Pd NP-supported mesoporous β-MnO_2 shows a new peak at 52°, which may be due to the stainless steel mesh. After discharge to 2.0 V, the peak at 25.4° still appears with a low intensity peak due to the teflonized acetylene carbon binder, but the peak at 35° may be due to the formation of Li_2O_2 and a peak at 52° still appears with low intensity due to stainless steel mesh. This result suggests that during the discharge process, the Au–Pd NP-supported mesoporous β-MnO_2 electrode shows the formation of Li_2O_2 after discharge to 2.0 V, but not the Li_2O. We previously reported that dispersion of Pd on the mesoporous β-

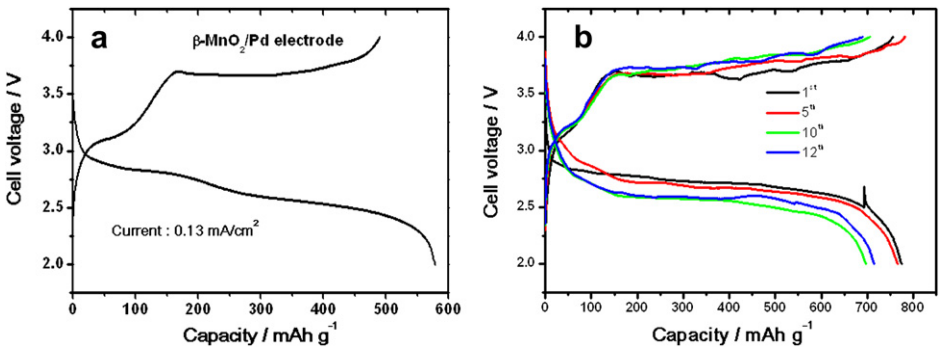

Fig. 4. Charge/discharge curves for a Li-Air battery using mesoporous β-MnO_2 supported palladium electrode and Au–Pd NP-supported mesoporous β-MnO_2 in an O_2 atmosphere between 4.0–2.0 V at a current density of 0.13 mA cm^{-2}. (a) Mesoporous β-MnO_2/Pd/TAB (75/15/10) electrode (b) Au–Pd NP-supported mesoporous β-MnO_2/TAB (90/10) electrode.

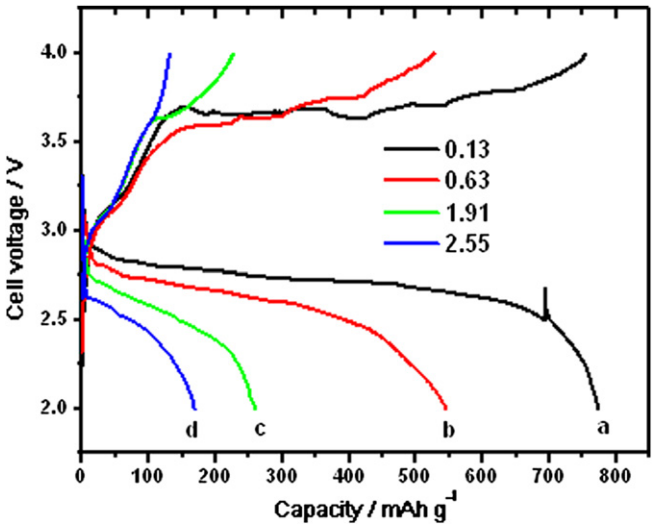

Fig. 5. First charge/discharge curves of (a) Au–Pd NP-supported mesoporous β-MnO_2/TAB (90/10) electrode at a current rate of (a) 0.13, (b) 0.65, (c) 1.91, and (d) 2.55 mA cm^{-2}.

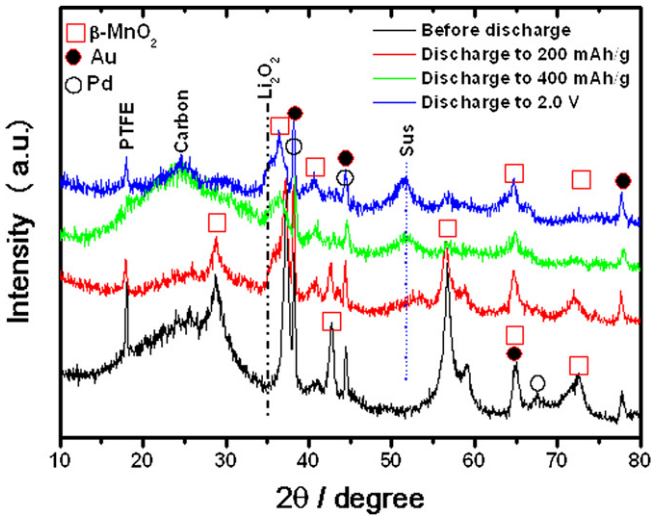

Fig. 7. *Ex-situ* XRD of Au–Pd NP-supported mesoporous β-MnO_2/TAB (90/10) electrode before discharge and after discharge to 200, 400 mAh g^{-1}, and 2.0 V.

MnO_2 air electrode for the Li-Air battery during the discharge process shows the formation of Li_2O_2 at high potential followed by Li_2O formation at 2.0 V [11]. In this study, *ex-situ* XRD results of Au–Pd NP-supported mesoporous β-MnO_2 electrode during discharge shows the formation of Li_2O_2, which is a similar reaction mechanism like the synthesis of H_2O_2 using Au–Pd catalyst [18,19].

Raman spectroscopy is one of the most useful techniques for measuring Li_2O_2 and Li_2O formation during discharge in the Li-Air battery. We also measured the *ex-situ* Raman spectroscopy of the Au–Pd NP-supported mesoporous β-MnO_2 air electrode for Li-Air battery before discharge, after discharge to 200, and 400 mAh g^{-1}, and after discharge to 2.0 V as shown in Fig. 8. Before discharge, *ex-situ* Raman spectroscopy of the Au–Pd supported β-MnO_2 air electrode showed different intensity peaks from each component, i.e., the peaks at 165 and 606 cm^{-1} correspond to Au, the peak at 526 cm^{-1} corresponds to Pd, and the peaks at 272 and 642 cm^{-1} relate to Mn. After discharge to 200 mAh g^{-1}, a new shoulder-like peak appeared at 745 cm^{-1}, which is assigned to Li_2O_2. While the cell discharged to 400 mAh g^{-1} and 2.0 V, it still retains the shoulder-like peak at 745 cm^{-1}, which corresponds to Li_2O_2 formation. However, we did not observe any Li_2O peaks while

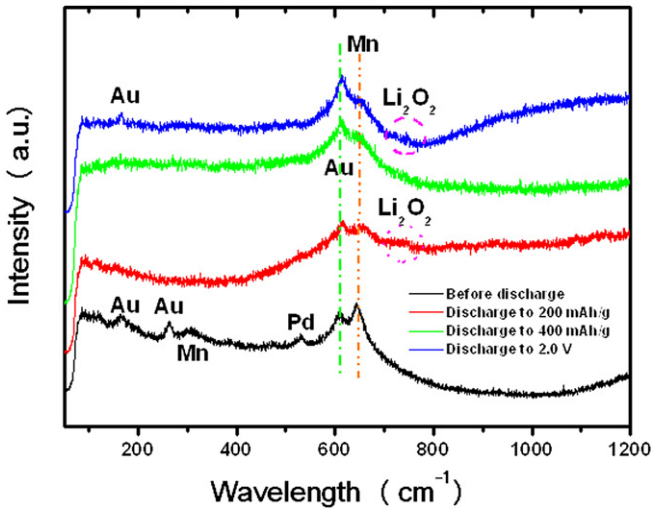

Fig. 8. *Ex-situ* Raman spectroscopy measurements of Au–Pd NP-supported mesoporous β-MnO_2/TAB (90/10) electrode before discharge and after discharge to 200, 400 mAh g^{-1}, and 2.0 V.

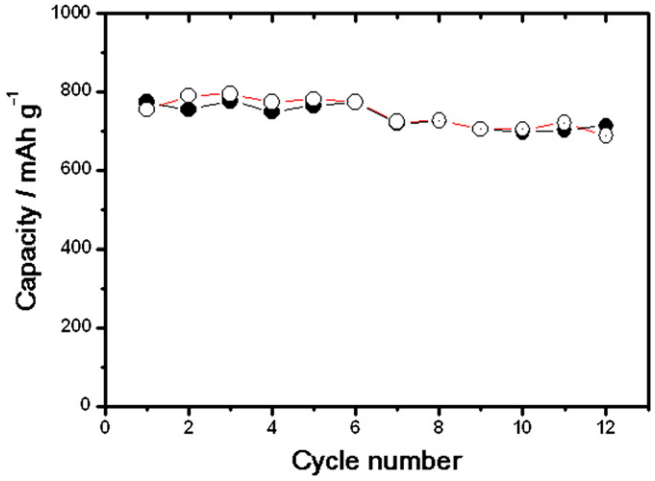

Fig. 6. Charge/discharge capacities versus cycle performance of Au–Pd NP-supported mesoporous β-MnO_2/TAB (90/10) electrode at a current rate of 0.13 mA cm^{-2}.

measuring *ex-situ* Raman spectroscopy of the Au–Pd NP-supported mesoporous β-MnO_2 cathode air electrode for the Li-Air battery. *Ex-situ* Raman spectroscopy measurement results suggested that the formation of Li_2O_2 only takes place in the case of the Au–Pd NP-supported mesoporous β-MnO_2 air electrode.

4. Conclusions

In summary, Au–Pd NP-supported mesoporous β-MnO_2 was successfully synthesized using a hydrothermal process. As a result, the catalytic activity of the Au–Pd NP-supported mesoporous β-MnO_2 cathode electrode enhanced the kinetics of ORR/OER with a high reversible capacity. A capacity of 775 mAh g^{-1} was achieved at the current density of 0.13 mA cm^{-2}. Further *ex-situ* XRD and Raman spectroscopy measurements of the Au–Pd NP-supported mesoporous β-MnO_2 cathode air electrode for the Li-Air battery suggest that formation of Li_2O_2 takes place during discharge and during charging while Li_2O_2 decomposed to Li^+ and O_2, which are reversible processes for Li-Air batteries.

Acknowledgments

This work was financially supported by Li-EAD project of the New Energy and Industrial Technology Development Organization (NEDO), Japan. The authors thank Andrew Marsh of the Conn Center for Renewable Energy Research at the University of Louisville for editing.

References

[1] K.M. Abraham, Z. Jiang, J. Electrochem. Soc. 143 (1996) 1–5.
[2] J. Read, J. Electrochem. Soc. 149 (2002) A1190–A1195.
[3] J. Read, K. Mutulo, M. Ervin, W. Behl, J. Wolfenstine, A. Driedger, D. Foster, J. Electrochem. Soc. 150 (2003) A1351–A1356.
[4] A. Debart, J. Bao, G. Armstrong, P.G. Bruce, J. Power Sources 174 (2007) 1177–1182.
[5] T. Ogasawara, A. Debart, M. Holfazel, P. Novak, P.G. Bruce, J. Am. Chem. Soc. 128 (2006) 1390–1393.
[6] A. Debart, A.J. Paterson, J. Bao, P.G. Bruce, Angew. Chem. Int. Ed. 47 (2008) 4521–4524.
[7] F. Mizuno, S. Nakanishi, Y. Kotani, S. Yokoishi, H. Iba, Electrochemistry 78 (2010) 403–405.
[8] F. Cheng, J. Shen, B. Peng, Y. Pan, Z. Tao, J. Chen, Nat. Chem. 3 (2011) 79–84.
[9] A.K. Thapa, K. Saimen, T. Ishihara, Electrochem. Solid-State Lett. 13 (2010) A165–A167.
[10] A.K. Thapa, T. Ishihara, J. Power Sources 196 (2011) 7016–7020.
[11] A.K. Thapa, Y. Hidaka, H. Hagiwara, S. Ida, T. Ishihara, J. Electrochem. Soc. 158 (2011) A1483–A1489.
[12] Y. Wan, D.Y. Zhao, Chem. Rev. 107 (2007) 2821–2860.
[13] L.Y. Song, D. Feng, N.J. Fredin, K.G. Yager, R.I. Jones, Q.Y. Wu, D.Y. Zhao, B.D. Vogt, ACS Nano 4 (2010) 189–198.
[14] F. Kleitz, S.H. Choi, R. Ryoo, Chem. Commun. 17 (2003) 2136–2137.
[15] T.W. Kim, F. Kleitz, B. Paul, R. Ryoo, J. Am. Chem. Soc. 127 (2005) 7601–7610.
[16] B.D. McCloskey, D.S. Bethune, R.M. Sheldy, G. Girishkumar, A.C. Luntz, J. Phys. Chem. Lett. 2 (2011) 1161–1166.
[17] A.M. Andersson, M. Herstedt, A.G. Bishop, K. Edstrom, Electrochim. Acta 47 (2002) 1885–1898.
[18] J. Li, A. Staykov, T. Ishihara, K. Yoshizawa, J. Phys. Chem. C 115 (2011) 7392–7398.
[19] J. Li, T. Ishihara, K. Yoshizawa, J. Phys. Chem. C 115 (2011) 25359–25367.